Available online at www.sciencedirect.com

ScienceDirect

Procedia Engineering 97 (2014) 854 – 863

Procedia Engineering

www.elsevier.com/locate/procedia

12th GLOBAL CONGRESS ON MANUFACTURING AND MANAGEMENT, GCMM 2014

Numerical Simulation of Temperature Distribution and Material Flow During Friction Stir Welding of Dissimilar Aluminum Alloys

R. Padmanaban [a]*, V. Ratna Kishore [b], and V. Balusamy[c]

[a, b] *Department of mechanical Engineering, AMRITA VISHWA VIDYAPEETHAM, Coimbatore- 641 112, Tamilnadu, INDIA*

[c] *Department of metallurgical Engineering, PSG College of Technology, Peelamedu, Coimbatore-641004, INDIA.*

Abstract

Joining dissimilar materials is required in many engineering applications and conventional fusion welding of dissimilar materials often results in defective welds. Friction Stir Welding (FSW) has paved way for joining dissimilar alloys and defect-free joints have been obtained for a number of dissimilar material combinations. Numerical modelling of FSW process can provide reasonable insight into the physics of the process and will aid in minimising the number of experimental trials. In this paper, Computational Fluid Dynamics (CFD) based numerical model is developed to predict the temperature distribution and material flow during FSW of dissimilar aluminum alloys AA2024 and AA7075. Volume of fluid approach is used and the FSW process is modelled as a steady-state visco-plastic laminar flow past a rotating cylindrical tool. Results indicate that peak temperature in the welded plates increases with the increase of Tool Rotation Speed (TRS) and Shoulder Diameter (SD), whereas the peak temperature decreases with increase in Welding Speed (WS). Increasing TRS and SD increases material flow, while increasing WS decreases material flow in the stir zone.

Selection and peer-review under responsibility of the Organizing Committee of GCMM 2014

Keywords: Friction Stir Welding; Computational Fluid Dynamics; Volume of Fluid; Temperature Distribution; Material flow.

* Corresponding author. Tel.: +91-9894568309; fax: +0422-2656274.
E-mail address: dr_padmanaban@cb.amrita.edu

Selection and peer-review under responsibility of the Organizing Committee of GCMM 2014
doi:10.1016/j.proeng.2014.12.360

1. Introduction

Friction Stir Welding (FSW), is a solid state joining process invented by the TWI, Cambridge in 1991[1]. In this process a cylindrical tool with a profiled probe is rotated and slowly plunged into the abutting edges of work pieces, until the shoulder of the tool touches the upper surface of the work pieces. The tool is then translated (with an axial force) along the length of the joint. Frictional heat generated due to the relative motion at the interface softens the material of the plates. The translation of the tool results in a visco-plastic flow of the material from the leading edge of the tool to the trailing edge and forms a joint in the solid state. As the process joins the materials at temperatures below the melting temperature of the base metal, problems occurring in the conventional welding process are eliminated. FSW finds application in ship building and marine industries, aerospace industries, automotive and railway industries [2, 3].

Nomenclature

R_P Tool pin radius
R_S Shoulder Radius
P_T Axial Pressure
δ Extent of Sticking
C_f Power Efficiency Factor
μ Friction Coefficient
U Traverse speed

The effect of process parameters and tool geometry on the heat transfer aspects and material flow has been studied by experimental and modeling approaches. Numerical modeling of friction stir welding has been used as a tool to explore the temperature field and to visualise material flow. In addition, numerical studies can assist one in understanding the FSW mechanism and avoiding process condition for which defects may occur. Modeling material flow in FSW has been accomplished using Lagrangean, Eulerian and Arbitrary Lagrangean Eulerian approaches. Eulerian models are based on CFD, with the results obtained by solving the equation of continuity, momentum and energy to obtain the required results. In Eulerian configuration, the results are analyzed either by the implementation of heat flux on the respective faces [4, 5] or by the viscous dissipation of the fluid due to the tool rotation [6, 7]. Modeling approach is fast and cost effective, but the results have to be validated by experimental data.

Colegrove and Schercliff [6, 8, 9] analysed material flow and temperature around tools and the forces acting on the tool during FSW using CFD based model. Long and Reynolds [7] used CFD based model to study the effect of material properties and process parameters on the x-axis force, material flow pattern and hence, potential defect formation. Nandan et al. [5] investigated heat transfer and visco-plastic material flow during FSW of aluminum alloy by numerically solving the equations of conservation of mass, momentum and energy in three dimensions using spatially variable thermo-physical properties and temperature, strain-rate dependent non-Newtonian viscosity. Crawford et al. [10] examined the effect of process parameter variation on forces & torques during FSW and mechanistic defect formation. Zhao et al. [11] simulated FSW of 2014 Al alloy using Eulerian formulation with coupled viscoplastic flow and heat transfer near the tool and predicted velocity field, temperature distribution, strain rate and micro hardness.

Colegrove et al. [12] presented a model for predicting heat generation in FSW from the material properties, tool and plate dimensions and the process parameters. Atharifar et al. [4] presented a CFD model for simulating material flow and heat transfer in the FSW of 6061-T6 aluminum alloy and analyzed the viscous and inertia loads applied to the tool by varying the welding parameters. With the pattern of material flow around the tool known for different process parameters, the formation of defects can be explained [13].

While FSW of similar materials has been explored by researchers, joining dissimilar materials by friction stir welding is a recent area of research with practical challenges and is gaining significant interest recently [14]. The 2xxx series and 7xxx series alloys possess high strength and low weight characteristics and are used in modern and future aircrafts. For example, the AA7075 plates are FS lap welded as skin with the AA 2024 stringers in aerospace

applications [15]. High strength, fatigue and fracture resistant joints in these alloys have been a challenge with the conventional processes. Hence technologies to join these alloys should be evaluated and studied. Friction stir welding has overcome these problems and these alloys have been successfully friction stir welded.

Very few studies have been conducted on dissimilar FSW of AA2024 and AA7075, the high strength aerospace aluminum alloys. Da Silva et al. [16] investigated the effect of joining parameters on the mechanical properties, microstructural features and material flow during friction stir welding of AA2024-T3 and AA7075-T6 dissimilar aluminum alloys. Cavaliere et al. [17] analysed the mechanical response, fatigue endurance and micro structural properties of AA2024-AA7075 joints fabricated by FSW. Khodir and Shibayanagi [18] studied the effect of welding speed and location of base metal on the microstructure and mechanical properties of dissimilar friction stir welded AA2024 and AA7075 joints. In this work CFD based model for the heat transfer and material flow during dissimilar friction stir welding of AA2024-AA7075 is developed using FLUENT. The aim of this work is to explore the effect of TRS, WS and SD on the thermal history, temperature distribution, and material flow during dissimilar FSW of aluminum alloys AA2024 and AA7075.

2. Friction Stir Welding Setup

Friction stir welding trials were made using a 3-axis vertical milling centre on AA2024 and AA7075 plates 150 mm long, 75 mm wide and 5 mm thick. The base metal plates were rigidly clamped to a low carbon steel backing plate, which was clamped to the machine bed as shown in “Fig.1”. High Speed Steel (HSS) taper threaded tools were used for welding and had a shoulder diameter of 17.5 mm, pin diameter of 5 mm and a pin height of 4.65 mm. The plates were friction stir welded in the butt configuration with the welding direction perpendicular to the rolling direction. AA2024 plates were placed on advancing side and the tool was rotated clockwise with respect to the vertical axis.

Figure 1 FSW setup showing work piece and Backing Plate

3. Numerical Modeling

The friction stir welding process is modeled as a steady-state visco-plastic laminar flow past a rotating tool. The isometric view of the meshed workpiece is shown in Fig. 2. The model is meshed with 551470 hexahedral cells using GAMBIT software. The region close to the faying surfaces is meshed with a fine cell size to increase the accuracy of the solution and the farther regions are meshed with a coarse size. The tool and fixing clamps are not included in the model. The pin and shoulder of the tool are inscribed in the workpiece and as the fluids that pass through the domain are different, the continuum is defined for both the sides. The face on the extreme end of the negative x-axis is defined as a velocity inlet with its opposite face defined as outflow. Rest of the faces of the work piece and the inscribed tool faces are defined as walls.

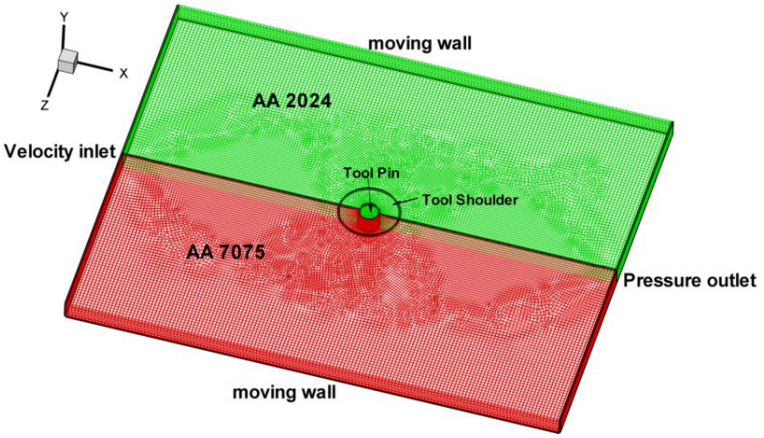

Figure 2 Isometric view of the grid and Boundary conditions

With fluids on both the sides, the face intermediate to both the fluids is defined as an interior. The faces of the tool on the advancing and retreating sides are defined separately to define the heat flux boundary condition according to the material on the advancing and retreating sides. A definite face separating the volumes enables the model to be solved in steady state with the Volume of Fluid (VOF) approach for dissimilar metals. Heat flux for the different regions of the tool are applied in the following manner.

The heat flux source at the shoulder matrix interface yields:

$$q_S = C_f[\delta\tau(\omega r - U\sin\theta) + (1-\delta)\mu P_T) \quad R_p \le r \le R_s . \tag{1}$$

When δ =1, full sticking is indicated and all heat is generated by plastic deformation. When δ = 0, heat is generated only by friction. The heat flux source for the vertical and horizontal surface of the tool pin is given by

$$q_v (= q_h) = C_f \tau(\omega r - U\sin\theta) \tag{2}$$

The temperature dependant shear stress τ is given by $\frac{\sigma_y}{\sqrt{3}}$. The work piece is translated along the positive x direction, i.e. fluid flows along the positive x direction and tool is rotated along the positive y direction. The material is endowed with the temperature dependent specific heat capacity, viscosity and thermal conductivity. Temperature dependent material properties were fed using UDF.

The heat transfer between the top surface of the workpiece and the surroundings beyond the shoulder is specified by convective boundary condition. Since convective heat losses occur across all free surfaces, convection co-efficient of 30 $Wm^{-2}\,K^{-1}$ was applied to the top and side surfaces of the work piece [19]. The contact conductance at the bottom surface, between the workpiece and backing plate is modeled by an enhanced heat transfer coefficient [20]. In this work a convection coefficient value of h = 350 $Wm^{-2}K^{-1}$ was applied to the bottom surface of the work piece. The boundary condition at the tool - workpiece interface is calculated from frictional heat. Since the temperature at the top surface of the work piece changes with respect to time, non uniform boundary conditions are defined as profile functions instead of constant values. The friction co-efficient μ is taken as 0.26 and the temperature dependent yield stress is hooked along with the viscosity of the material. Second order upwind scheme is used for solving the governing equations.

The velocity at the tool pin periphery and shoulder has been defined in terms of tool translational velocity and the tool pin angular velocity. At all other surfaces, temperatures are set at ambient temperature and velocities are set to zero. The temperature dependent material properties considered in the present work can be found in [3, 5, 21-26]. The model is validated by using it for simulating dissimilar FSW of AA5083-AA6082 with a TRS of 840 rpm and WS of 100 mm/min. Fig.3 compares transient temperature obtained from the present simulation and experimental

results measured by Peel et al. [27]. The difference between the measured and computed temperature at the end of the welding is due to assumption of convective boundary condition for the backing plate in the model.

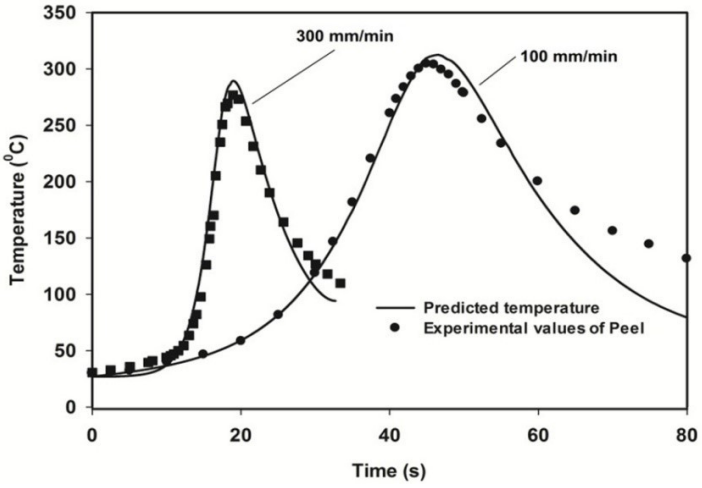

Figure 3 Comparison of simulated temperatures with Peel and Steuwer [27]

4. Results

The heat generated during FSW must be sufficient enough to soften, stir and mix the material. The computed temperature profiles along the top surface of the workpiece and transverse sections through the tool axis are shown in Fig.4, Fig.5 and Fig.6.

4.1. Effect of Welding Speed

The temperature contours on transverse cross section obtained during FSW of AA7075 and AA2024 at various Welding Speeds (WS) are shown in Fig. 4. The tool rotation speed is maintained at 900 rpm and shoulder diameter is 17.5 mm. From the Fig.4, It is seen that the peak temperature decreases with increase in WS. As the WS increases from 20 mm/min to 60 mm/min, the temperature drops from 726 to 704 K. This happens due to the reduced heat input per unit length and dissipation of heat over a wider region of workpiece at higher WS. When the WS is low, the material in front of the tool is subjected to higher temperatures. This results in the tool, stirring material that is softened due to increased temperature thus reducing the forces acting on the tool. When the WS is high, the material in front of the tool is subjected to low temperatures, resulting in the tool stirring a comparatively harder material, increasing the forces acting on the tool. This will affect the tool life [28].

4.2. Effect of tool rotation speed

The temperature distributions on transverse section obtained during FSW of AA7075 and AA2024 for different tool rotation speed (TRS) are shown in Fig.5. The WS and SD are 20 mm/min are 17.5 mm respectively. When the TRS is 900 rpm, the peak temperature is 726K, which increases to 739K and 745K when the tool rotation is increased to 1050 and 1200 rpm respectively. Increase in TRS has caused a significant increase in the peak temperature, because of the increase in heat generation from higher rotational speeds. The increase in temperature with increase in TRS decreases at higher TRS, because the material properties decrease as the material temperature increases. Thus, continuous increase in TRS will not result in continuous increase in peak temperature, and hence the maximum temperature during FSW is about 80-90% of the base material melting point [29, 30].

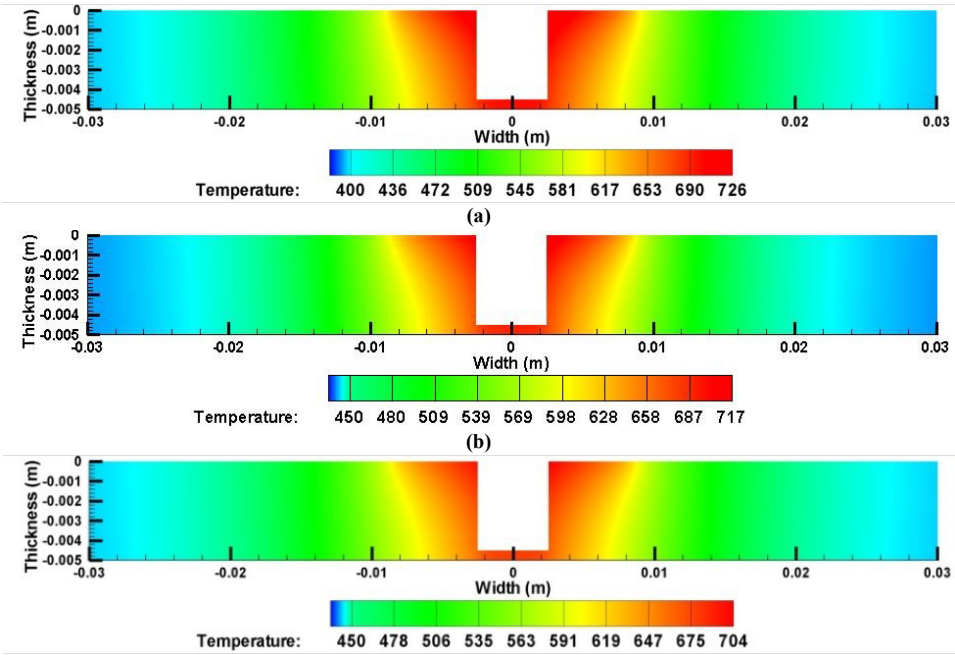

Figure 4 Temperature contours on transverse section for WS of a) 20 mm/min b) 40 mm/min and c) 60 mm/min. SD =17.5 mm, TRS =900 rpm.

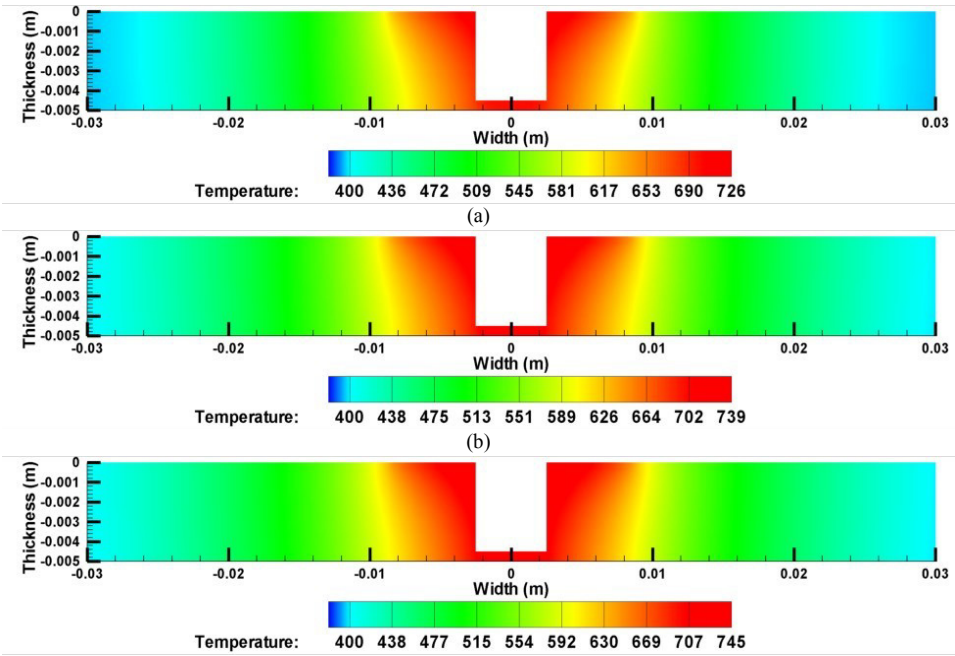

Figure 5 Temperature contours on transverse section (a) 900 rpm (b) 1050 rpm and (c) 1200 rpm. WS =20 mm/min and SD=17.5 mm

4.3. Effect of Parameters on Stir Zone Size

The shape of the isoviscosity contour can correlate well with boundaries of stirring zone. The viscosity contours up to the order of $5x10^6$ kg-m/s, correspond to the viscoplastic flow region for aluminum alloys [5]. The variation of viscosity due to change in TRS, WS and SD on transverse sections are presented in Fig.6, Fig.7 and Fig.8.

From Fig.6, it can be observed that increasing the TRS increases the size of the stir zone. Increasing the TRS from 900 rpm to 1200 rpm, causes the minimum viscosity in the stirred zone to decrease from 48076.2 to 35318.2 Pa-s. The SD and WS are 17.5 mm and 20 mm/min respectively. This will enable material flow, efficient mixing. In addition to the above, the forces acting on the tool will be less as the material offers less resistance.The variation of viscosity due to change in SD is shown in Fig.7. When SD is increased from 15 mm to 20 mm, the minimum viscosity in the stirring zone decreases from 43100 to 40351Pa-s. The TRS and WS are 900 rpm and 20 mm/min respectively. When the SD is increased, the stirring zone size increases indicating that the material flow is enhanced. When the SD is 20 mm the size of the stirred zone at the bottom of the plate is also increased. The effect of WS on the viscosity in the stirring zone is depicted in Fig.8. The TRS and SD are 900 rpm and 17.5 mm respectively. When WS is increased, the stirring zone size decreases, indicating that the material flow is affected when WS is increased. It can be noted that increasing the welding speed from 20 mm/s to 60 mm/s at a constant TRS of 1050 rpm and SD of 17.5 mm increases the minimum viscosity in the stir zone from 40351.3 to 47592 Pa-s. This indicates that the material would offer comparatively more resistance to tool movement and material mixing will not be efficient at higher welding speeds**.**

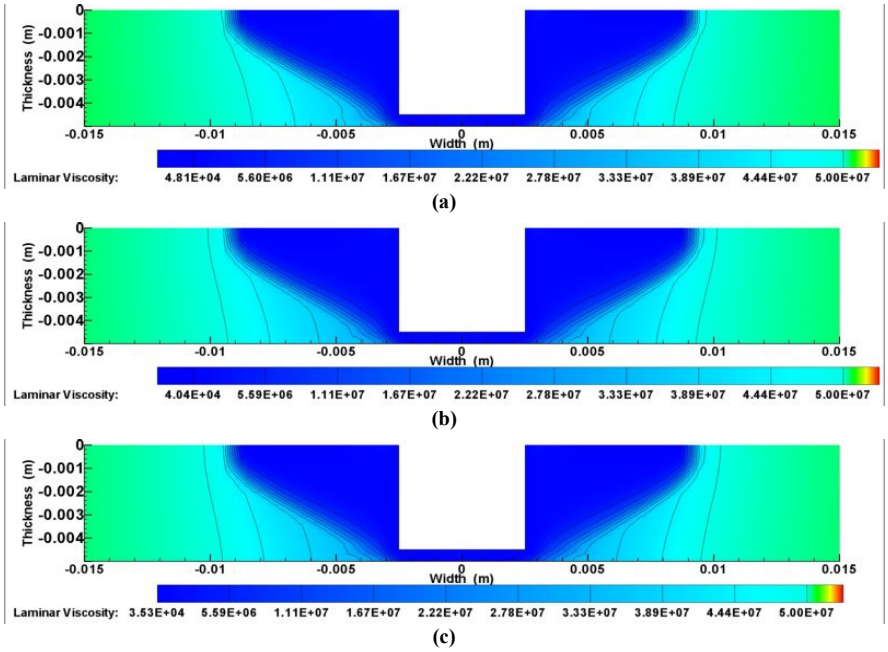

Figure 6 Contour plots of viscosity at TRS of a) 900 rpm, b) 1050 rpm and c) 1200 rpm, WS=20 mm/min, SD=17.5 mm

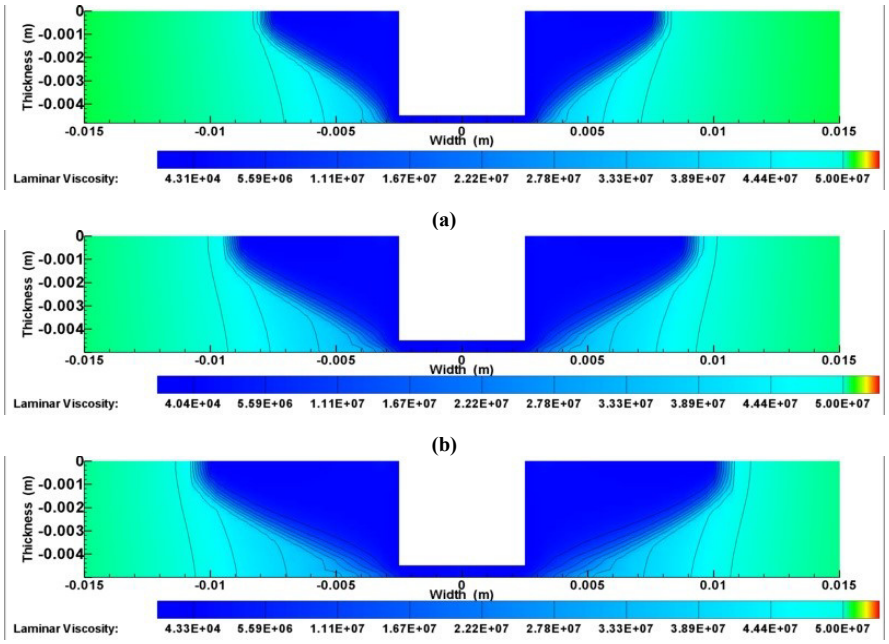

Figure 7 Contour plots of viscosity at SD of a) 15 mm, b) 17.5 mm and c) 20 mm. WS=20 mm/min, TRS=1050 rpm

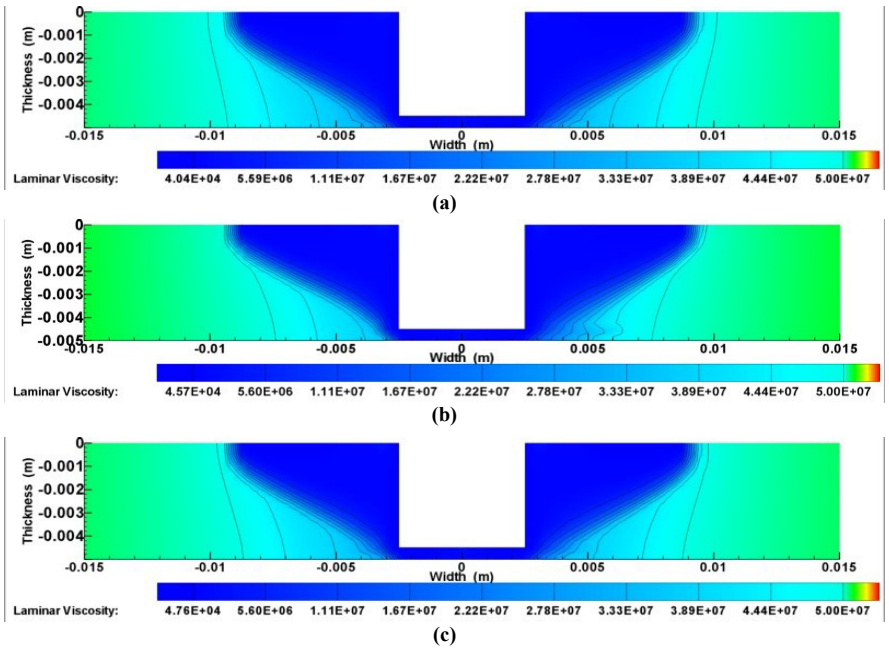

Figure 8 Contour plots of viscosity at WS of a) 20 mm/min, b) 40 mm/min and c) 60 mm/min. TRS=1050 rpm , SD=17.5 mm

5. Conclusions

CFD based model for the heat transfer and material flow during dissimilar friction stir welding of AA2024-AA7075 is developed. The temperature distribution is found to be asymmetric and the maximum temperature reached is between 80 to 90% of the liquidus temperature of material welded. The temperature distribution in FSW is affected by both TRS and WS. Specifically increasing TRS increases peak temperature during FSW, while peak temperature decreases with increase in WS. Increasing TRS increases tool life and enhances material mixing, while increasing WS increases loads acting on the tool and hence affects life of the tool. Similarly increasing TRS and SD decreases the viscosity in the nugget region, enhancing material flow. Increasing WS affects material flow as observed from higher viscosity in the stir zone.

References

[1]. Thomas, W.M., et al., Friction Stir Butt Welding. 1991, The Welding Institute,Cambridge,UK.
[2]. Mishra, R.S. and Z.Y. Ma, Friction stir welding and processing. Materials Science and Engineering: R: Reports, 2005. 50(1-2): p. 1-78.
[3]. Nandan, R., T. DebRoy, and H.K.D.H. Bhadeshia, Recent advances in friction-stir welding - Process, weldment structure and properties. Progress in Materials Science, 2008. 53(6): p. 980-1023.
[4]. Atharifar, H., D. Lin, and R. Kovacevic, Numerical and Experimental Investigations on the Loads Carried by the Tool During Friction Stir Welding. Journal of Materials Engineering and Performance, 2009. 18(4): p. 339-350.
[5]. Nandan, R., G. Roy, and T. Debroy, Numerical simulation of three-dimensional heat transfer and plastic flow during friction stir welding. Metallurgical and Materials Transactions A, 2006. 37(4): p. 1247-1259.
[6]. Colegrove, P.A. and H.R. Shercliff, 3-Dimensional CFD modelling of flow round a threaded friction stir welding tool profile. Journal of Materials Processing Technology, 2005. 169(2): p. 320-327.
[7]. Long, T. and A.P. Reynolds, Parametric studies of friction stir welding by commercial fluid dynamics simulation. Science and Technology of Welding & Joining, 2006. 11(2): p. 200-208.
[8]. Colegrove, P.A. and H.R. Shercliff, Development of Trivex friction stir welding tool Part 1 ; two-dimensional flow modelling and experimental validation. Science and Technology of Welding & Joining, 2004. 9(4): p. 345-351.
[9]. Colegrove, P.A. and H.R. Shercliff, Development of Trivex friction stir welding tool Part 2 ; three-dimensional flow modelling. Science and Technology of Welding & Joining, 2004. 9(4): p. 352-361.
[10]. Crawford, R., et al., Experimental defect analysis and force prediction simulation of high weld pitch friction stir welding. Science and Technology of Welding and Joining, 2006. 11: p. 657-665.
[11]. Zhao, Y.H., et al., Microhardness prediction in friction stir welding of 2014 aluminium alloy. Science and Technology of Welding & Joining, 2006. 11(2): p. 178-182.
[12]. Colegrove, P.A., H.R. Shercliff, and R. Zettler, Model for predicting heat generation and temperature in friction stir welding from the material properties. Science and Technology of Welding & Joining, 2007. 12(4): p. 284-297.
[13]. Long and Reynolds.A.P, Parametric studies of friction stir welding by commercial fluid dynamics simulation. Science and Technology of Welding and Joining, 2006. 11: p. 200-208.
[14]. DebRoy, T. and H.K.D.H. Bhadeshia, Friction stir welding of dissimilar alloys; a perspective. Science and Technology of Welding & Joining, 2010. 15(4): p. 266-270.
[15]. Bahemmat, P., et al., Study on dissimilar friction stir butt welding of AA7075-O and AA2024-T4 considering the manufacturing limitation. The International Journal of Advanced Manufacturing Technology, 2012: p. 939-953.
[16]. Da Silva, et al., Material flow and mechanical behaviour of dissimilar AA2024-T3 and AA7075-T6 aluminium alloys friction stir welds. Materials & Design, 2011. 32(4): p. 2021-2027.
[17]. Cavaliere, P., et al., Mechanical and microstructural behaviour of 2024–7075 aluminium alloy sheets joined by friction stir welding. International Journal of Machine Tools and Manufacture, 2006. 46(6): p. 588-594.
[18]. Khodir, S.A. and T. Shibayanagi, Friction stir welding of dissimilar AA2024 and AA7075 aluminum alloys. Materials Science and Engineering: B, 2008. 148(1-3): p. 82-87.
[19]. Khandkar, M.Z.H., J.A.Khan, and A.P.Reynolds, Prediction of temperature distribution and thermal history during friction stir welding: input torque based model. Science and Technology of Welding and Joining, 2003. 8: p. 165-174.
[20]. Chen, C.M. and R. Kovacevic, Finite element modeling of friction stir welding—thermal and thermomechanical analysis. International Journal of Machine Tools and Manufacture, 2003. 43(13): p. 1319-1326.
[21]. Nandan, R., et al., Numerical modelling of 3D plastic flow and heat transfer during friction stir welding of stainless steel. Science and Technology of Welding & Joining, 2006. 11(5): p. 526-537.
[22]. Nandan, R., et al., Three-dimensional heat and material flow during friction stir welding of mild steel. Acta Materialia, 2007. 55(3): p. 883-895.
[23]. Ulysse, P., Three-dimensional modeling of the friction stir-welding process. International Journal of Machine Tools and Manufacture, 2002. 42(14): p. 1549-1557.

[24].Dong, P., et al., Coupled thermomechanical analysis of friction stir welding process using simplified models. Science and Technology of Welding & Joining, 2001. 6(5): p. 281-287.
[25].Heurtier, P., et al., Mechanical and thermal modelling of Friction Stir Welding. Journal of Materials Processing Technology, 2006. 171(3): p. 348-357.
[26].Ian Mitchell, Residual stress Reduction During Quenching of Wrought 7075 Aluminum alloy, in Department of Material Science and Engineering. 2004, Worcester Polytechnic Institute.
[27].Peel, M., et al., Dissimilar friction stir welds in AA5083-AA6082. Part I: Process parameter effects on thermal history and weld properties. Metallurgical and Materials Transactions A, 2006. 37(7): p. 2183-2193.
[28].Chao, Y.J., X. Qi, and W. Tang, Heat Transfer in Friction Stir Welding---Experimental and Numerical Studies. Journal of Manufacturing Science and Engineering, 2003. 125(1): p. 138-145.
[29].Tang, W., et al., Heat Input model and temperature distribution in friction stir welding. Journal of Material Processing and Manufacturing Science, 1998. 7: p. 163-172.
[30].Colegrove, P.A. and H.R. Shercliff, Experimental and numerical analysis of aluminium alloy 7075-T7351 friction stir welds. Science and Technology of Welding & Joining, 2003. 8(5): p. 360-368.